Highly sensitive temperature-independent FBG-based sensor embedded in thermoplastic polyurethane using 3D printing technology for the measurements of torsion

Mohamad Ashraff Alias [a], Harith Ahmad [a,d,*], Muhamad Zharif Samion [a], Muhammad Syamil Mohd Sa'ad [a], Lim Kok Sing [a], Kenneth T.V. Grattan [b], B.M. Azizur Rahman [b], Gilberto Brambilla [c], Muhammad Khairol Annuar Zaini [a], Leonard Bayang [a], Mohammad Faizal Ismail [a]

[a] *Photonics Research Center, Universiti Malaya, 50603 Kuala Lumpur, Malaysia*
[b] *School of Mathematics, Computer Science & Engineering, City, University of London, London EC1V 0HB, United Kingdom*
[c] *Optoelectronics Research Center, University of Southampton, Southampton SO17 1BJ, United Kingdom*
[d] *Adjunct Professor, Department of Physics, Universitas Negeri Malang, Jalan Semarang 5, Malang 65145, Indonesia*

A B S T R A C T

A new design of optical Fiber Bragg Grating (FBG)-based sensor for the measurement of torsion (twist) has been developed, which, while offering a high level of accuracy, can be fabricated inexpensively using 3D printing technology. In this sensor design, an FBG is embedded inside the thermoplastic polyurethane (TPU) filament, which acts as the sensing pad for the FBG, taking advantage of its highly elastic properties and excellent sensitivity to variations in local strain. Experiments conducted have shown that the embedded FBG-based sensor can be used effectively in the measurements of torsion or rotation, at a bonding angle of 45°, giving an average responsivity of 0.95 pm/deg in both the clockwise and anticlockwise direction over the range of − 100° to + 100°, with good linearity of up to 99%. Furthermore, the device has been developed to allow for the effects of any temperature changes to be compensated by including an additional but 'untwisted' FBG in the sensor design. It provides a temperature sensitivity of 18.90 pm/°C. This design of twist measurement sensor described in this work also shows a good response in the underground soil movement, giving an average responsivity of 0.95 pm/deg in both the clockwise and anticlockwise direction over the range of − 100° to + 100°, with good linearity of up to 99%. This proves that this fabricated device can be made applicable to a wide range of engineering applications reliably and inexpensively.

1. Introduction

The rapid advancement of fiber optic sensors has given rise to extensive research and development due to their outstanding performance and versatility in various environments. They show several distinctive advantages over the conventional sensors available in today's market, taking advantage of their immunity to external electromagnetic fields [1], their relative ease of installation [2] due to their small size and flexibility [3], their significant corrosion resistance [4], as well as the ready availability [5] in the market of a wide range of optical fiber types and components. Fiber Bragg Grating (FBG)-based optical sensors have developed in recent years to be amongst the most broadly applied fiber optic sensors across a wide range of in-the-field applications, taking advantage of their compact size and lightweight nature [6] and their multiplexing capabilities [7,8]. On top of this is their potential for quasi-distributed monitoring of different systems [9,10], potentially offering higher sensitivity as well as being chemically inert [10], which is essential for some specific applications. Furthermore, it can be designed for continuous long-distance remote monitoring [11–13], taking advantage of its high-speed response [14], which can offer both cost and time-effective solutions to many different measurement processes.

By applying the wavelength-encoded properties of the FBGs in a fiber-optic network, accurate measurements of strain, tilt, pressure,

Table 1
Comparison with other 3D printed sensors based on FBG.

Ref	Type of Sensor	Embedment Methods	Sensitivity Value
[22]	Tilt sensor	• No embedment • FBG is left bare and hung parallel to the shafts of the sensor	10.00 pm/deg of tilt
[29]	Strain sensor	• FBG is inserted in a 3D-printed TPU material • FBG is fixed using cyanoacrylate superglue	1.20 pm/$\mu\varepsilon$
[15]	Pressure sensor	• FBG is embedded directly in the 3D-printed material • FBG is laid in a special groove halfway during printing to be embedded	13.22 pm/kPa
[This work]	Torsion sensor	• FBG is inserted inside a 3D-printed TPU material • FBG is fixed using cyanoacrylate superglue	0.95 pm/deg of rotation

Fig. 1. Illustration of the dimensions of the embedded FBG-based sensor used in this work.

displacement, temperature, torque, and other physical parameters can be achieved [1,2,11,15]. Cross sensitivity, e.g., for a temperature effect is a feature of many such FBG-based sensors [16], and thus the design of the sensing element must ensure that compensation is provided [17]. This is to allow the simultaneous measurement of two parameters, such as strain and temperature. When fabricating FBGs in various fibers for different applications, different dopants [18] and fiber diameters [19] can facilitate the best use of discrimination of the strain and temperature effects experienced. The downside can be the added complexity of the sensor design.

Torsional measurements have been important to researchers due to their wide range of engineering applications – often together with temperature variations. In previous work, Xu et al. [20] have developed a stretchable Fiber Bragg Grating-based torsion sensor based on the sinusoidal embedding of an FBG in a silicone film. The twisting of the silicone film changes the effective FBG grating length, which causes a consequent shift in the Bragg wavelength. However, this approach has its drawbacks as it does not include a temperature compensation mechanism to allow for any temperature effects that the system experiences. It is also hard to implement a design of this type in large-scale field applications due to the requirement for the FBG to be embedded in such a structure. Chen et al. [21] also reported designing an optical torsion sensor based on tilted fiber Bragg gratings (TFBGs). Here, the TFBG was fabricated with the grating tilted at 81°, allowing the coupling of light from core to core to forward-propagating cladding modes. By this means, the direction of the torsional effect can be determined using an intensity demodulation technique. However, this method also has the problem that no temperature compensation mechanism has been included to enable correction for temperature effects.

This work developed a low-cost, temperature-independent FBG-based torsion sensor embedded in a 3D printed structure taking advantage of the proposed design's ease of fabrication [22,23]. Previous work by Ismail et al. [22] had demonstrated the use of 3D printing

technology to create a biaxial sensor system for measurements of tilt, based on the use of four fiber Bragg grating (FBG) tilt sensors which were fabricated using polylactic acid (PLA) material. Another work by Zhang et al. [15] also implemented the use of 3D printing where an FBG was embedded directly in a PLA material for measurements of vertical pressure. Alias et al. [23] also reported using 3D printing technology where an FBG-based extensometer system was developed by embedding the FBGs inside thermoplastic polyurethane (TPU) material to allow measurements of ground displacement to be taken. Table 1 shows the comparison between other 3D printed sensors in terms of their types, embedment methods, and sensitivity value. Other examples of embedment configurations are by using polydimethylsiloxane (PDMS) or dragon skin materials. There have been reports of using these materials to embed the FBGs into 3D printed materials due to their inexpensiveness, wide range of materials available, and ease of fabrication that have the capabilities to meet the demands of many applications [24–26]. Although PDMS can withstand high temperatures and are not affected by chemicals or UV radiations, it is still expensive and complicated when manufacturing it which will take some cost and time when compared to 3D printed embedment method. Another work by Lo Presti et al. [26] had shown the use of Dragon skin material to embed the FBG in the production of a wearable flexible FBG sensor for measurements of chest wall displacement in cardiac monitoring. However, similar to PDMS, this embedment configuration requires a complex manufacturing method in which the material needs to be mixed and cured at a specific temperature and requires a longer time for it to be fabricated. Therefore, we have chosen to embed our FBG in a 3D-printed structure due to its advantages. This work's design comprises four FBGs (with non-identical Bragg wavelengths) that are bonded along the surface of a circular structure containing a PVC pipe set at a specific angle. The experimental results have shown that the sensor can achieve torsion measurements over the wide (angular) range (of −100° to +100°) with a high level of precision. In the design, to provide correction for temperature effects, an additional FBG placed loosely inside the PVC pipe has been used to allow the separation of the strain and temperature effect seen. In the study carried out, the device was characterized over the temperature range from 25 °C to 50 °C to ensure that it can be used in various field applications, including structural health monitoring of engineering structures [26] and landslides [27].

2. Sensor structure and its principle

2.1. FBG-based sensor design

The design, including the dimensions of the embedded FBG sensor, is shown in Fig. 1. It illustrates an FBG embedded inside thermoplastic polyurethane (TPU) material, that was fabricated using 3D printing technology. The TPU material used was specifically engineered by *Ultimaker* to work on most desktop 3D printers, which in our case is the *Ultimaker 2 +* 3D printer with a filament diameter of 2.85 mm. TPU was selected as the sensor body due to its high flexibility and durability [10, 23,28] compared to other filaments, also known as 'printer inks' in 3D printing. This was due to its excellent shore hardness of 95 A, allowing the TPU structure to be stretched more than 3 times its original length. In
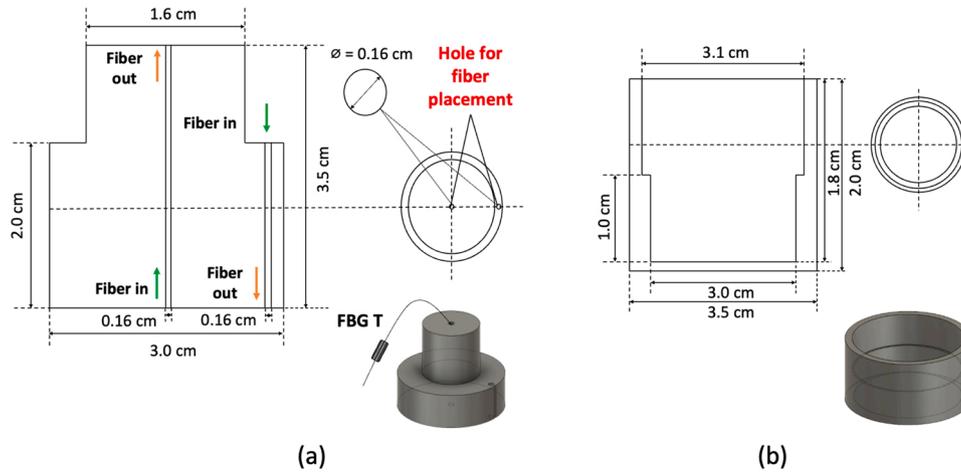
Fig. 2. Illustration of the dimensions of (a) the temperature compensation joint with FBG T and (b) the protective joint cap.

addition, the ability of this material to be stretched and compressed are more significant when compared to other available filaments, such as polylactic acid (PLA) [29] or acrylonitrile butadiene styrene (ABS) [28], thereby making it better suited to withstand significant tensile and compressive forces. Another benefit of using TPU as a material is its high strain sensitivity, compared to other available filaments, making it well suited to torsional strain measurements on circular structures [30], such as beams and pipes.

In this work, to optimize the sensor, the sensor element, which is the FBG was designed to be embedded at the center of a cuboid-shaped structure and has dimensions of 40 mm × 1.4 mm×1.4 mm, with an infill density of 20%. As infill density increases, the stiffness of the material also increases, thus limiting its flexibility during stretching which will result in a lower strain sensitivity. Furthermore, infill patterns also affect the performance of the 3D-printed structure. For example, a concentric infill pattern provides an excellent advantage in terms of flexibility, strength, and preparation time as its internal structure is composed of concentric lines that match the outline of the print. Grid or tri-hexagon infill patterns, on the other hand, contain an assortment of lines in each print layer which provides better strength in two dimensions but has lesser flexibility despite it taking a long time to fabricate. Moreover, as shown in Fig. 1, the sensor has been designed with a thin base, also known as the brim, at the bottom to allow more excellent bed adhesion to the circular structure of the pipe used. Since this sensor design was small and thin, about 1.4 mm thick, the infill pattern would not have much effect on the printed output, hence showing that any infill pattern can be applied as long as the density was not high. As such, the concentric infill pattern was chosen with a density of 20% as mentioned earlier. In addition, the vertical resolution was set to 0.10 mm, to establish a smooth layer thickness for the printed TPU structure. Taking advantage of the properties of the TPU material, the 3D printer printing speed was tuned at 40 mm/s using the Cura 3D printer software to ensure a smooth print output. Subsequently, the FBG was pre-stressed by pulling the ends of each of the FBG fibers before fixing them in place using cyanoacrylate glue. During this process, the FBG was first positioned through the printed holes (Ø = 0.12 cm) and taped to prevent any movements of the fiber during the gluing process.

2.2. Temperature compensation of the sensor system

In order to correct any temperature effects experienced by the sensor system, a further FBG, labeled as FBG T, has been integrated into this design. This additional FBG was fixed inside the PVC pipe through a 3D-printed protective casing to ensure that the FBG was well protected during the measurements. Fig. 2(a) illustrates the dimensions of the FBG T joint, fabricated using a PLA filament with an infill density of 30% and

a grid infill pattern. It is then placed at the rigid point of the PVC pipe. As shown in the figure, the fiber was inserted through the holes of the FBG T joint, causing the FBG T to be loosely fitted inside the PVC pipe and thus free from any strain variations. This arrangement allows FBG T to measure the temperature dependence alone, thus allowing any temperature effects present in the system to be monitored, and a temperature correction can be applied. Subsequently, another 3D printed cover fabricated using PLA material was used to seal the FBG T joint in place, to enable it to be used during measurements. Fig. 2(b) illustrates the design of the FBG T joint cap used in this work.

2.3. FBG sensing principle based on this design

The FBG forming the basis of the FBG-based sensors was of a uniform, positive-only index change type with a reflectivity of ≥ 90% and a grating length of 10 mm. These FBGs were fabricated using a typical SMF-28 fiber in our laboratory in which the polymer was removed from a section of the optical fiber, as to allow the FBG to be written at the core of the SMF-28 optical fiber using the phase mask technique. The buffer coating material of the FBGs is made of acrylate to allow a good temperature sensitivity of the FBG. A previous study by Razali et al. [31] had shown that acrylate-buffered FBG is 1.27 times more sensitive than bare FBG due to the higher thermal expansion of the acrylate buffer. This was also due to acrylate not being moisture sensitive and only sensitive towards temperature when compared to the other typical coating materials such as polyimide, which is not only costly but also sensitive to both moisture and temperature [32]. The interest of this sensor was to avoid unnecessary water absorption which will change the sensor's length and make it harder to compensate for temperatures, especially when used in field applications that are exposed to water environments such as in landslides monitoring. Acrylate was chosen as the buffer material to avoid the above problems. The FBGs used were not recoated as it was meant to be encapsulated inside a TPU material, whereby the FBG was fixed using cyanoacrylate glue. Fundamentally, when light from a broadband source was coupled into the fiber, the periodic change of the FBG gratings forming the torsion sensor was reflected, this being a narrow spectral part of the light at a particular wavelength (with the rest being transmitted). This reflected light forms a narrow band centered on the Bragg wavelength (λ_B), as given by Eq. (1):

$$\lambda_B = 2n_{eff}\Lambda \tag{1}$$

where λ_B is the Bragg wavelength that will be reflected, n_{eff} is the effective index of the optical fiber and Λ represents the FBG periodicity. The strain-temperature cross-sensitivity of such an FBG-based sensor is reflected if there is a change in the Bragg wavelengths, λ_B (this comes
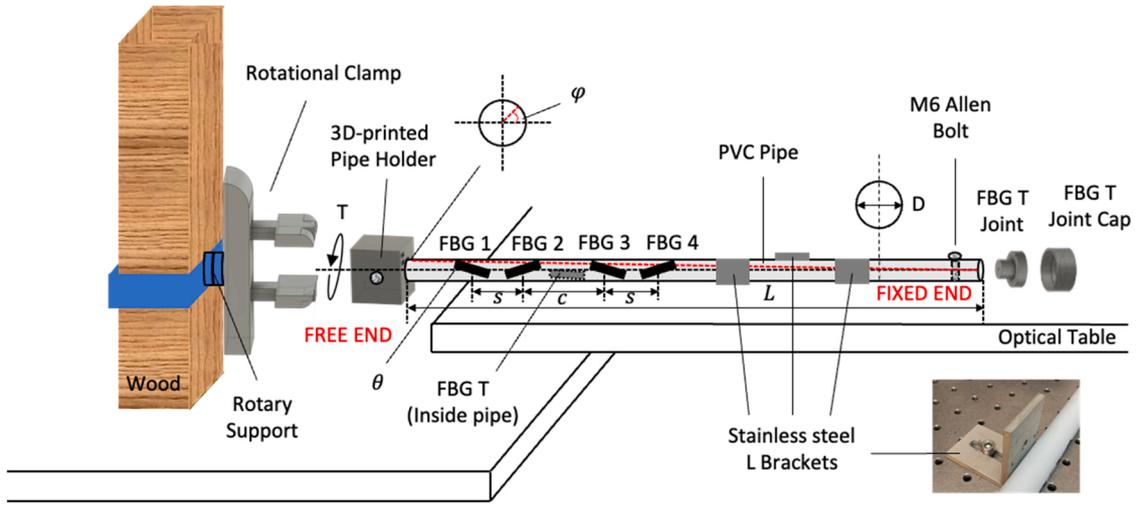
Fig. 3. Illustration of the design of the FBG-based sensor system for measurements of twist showing the strain-sensitive FBGs (FBG 1, 2, 3, and 4) with s = 6 cm (distance between FBG 1 and FBG 2, and FBG 3 and FBG 4) and c = 10 cm (distance between FBG 2 and FBG 3) as well as the incorporation of a strain-insensitive FBG (FBG T) inside the PVC pipe for temperature compensation.
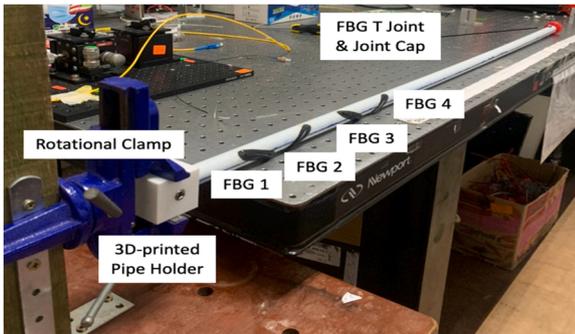
Table 2
FBG positions, their respective Bragg wavelengths, and bonding angle.

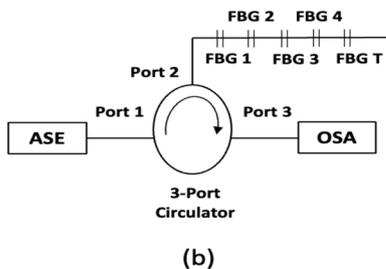| FBG #	Bragg Wavelength (nm)	Position Along The Pipe (cm)	Angle (°)
1	1539.0	92.0	30.0
2	1544.0	86.0	150.0
3	1549.0	76.0	30.0
4	1554.0	70.0	150.0
T	1559.0	Inside the pipe	–

Table 3
FBGs positions, their respective Bragg wavelengths, and different bond angles.

FBG #	Bragg Wavelength (nm)	Position Along The Pipe (cm)	Angles (°)
1	1539.0	92.0	45.0 and 60.0
2	1544.0	86.0	135.0 and 120.0
3	1549.0	76.0	45.0 and 60.0
4	1554.0	70.0	135.0 and 120.0
T	1559.0	Inside the pipe	–

$$\frac{\Delta\lambda_B}{\lambda_B} = \left(1 - p_{eff}\right)\Delta\varepsilon + (\alpha + \xi)\Delta T \qquad (2)$$

where $\Delta\lambda_B$ is the shift in the Bragg wavelength, p_{eff} represents the photoelastic parameter, $\Delta\varepsilon$ the strain variations experienced, α the coefficient of thermal expansion of the fiber material, and ξ the thermo-optic coefficient of the fiber, and ΔT represents the temperature changes. In order to provide temperature compensation to the whole sensor system, the strain-free FBG is labeled as FBG T, where $\Delta\varepsilon = 0$ in Eq. (2), and is placed loosely inside the PVC pipe. By this method, the temperature effects can be corrected, allowing the measurements of strain alone to be extracted. Although it was found that FBGs that are placed at opposite angles could be used for temperature compensation, the number of FBGs used will be higher. Instead, our proposed setup only used one FBG for temperature compensation, thus reducing the overall cost and providing simplicity.

In this work, the embedded FBG sensors incorporated into the sensor system are shown schematically in Fig. 3. Initially, when a torsion effect, T, is applied at the free end of the PVC pipe in the counterclockwise direction, the gratings labeled FBG 1 and FBG 3 will be stretched with both experiencing tensile strain, which will also cause the Bragg wavelength of both FBGs to experience a redshift – shifting to longer wavelengths ($\Delta\lambda_B > 0$). By contrast, FBG 2 and FBG 4 experience compressive strain (as both FBGs are compressed). This will cause their Bragg wavelength to experience a blueshift to shorter wavelengths ($\Delta\lambda_B < 0$). A similar approach can be applied when T is in the clockwise direction. Hence, the strains, ε_n, monitored by the FBGs, are given by [33,34]:

$$\varepsilon_n = \frac{1}{2}\gamma sin\theta_n \quad , (n = 1, \ 2, \ 3 \ \text{and} \ 4) \qquad (3)$$

(a)

(b)

Fig. 4. Illustration of (a) the experimental setup for measurements of twist and (b) a schematic diagram of the interrogation system for the FBGs used (FBG 1 to FBG 4) and FBG T (for temperature measurement).

from both the effects of the strain on the fiber and the thermal expansion (or contraction) effects, all this causes a change in the FBG grating periodicity, Λ. Hence, the Bragg wavelength observed from the FBG can be shown to be [20]:
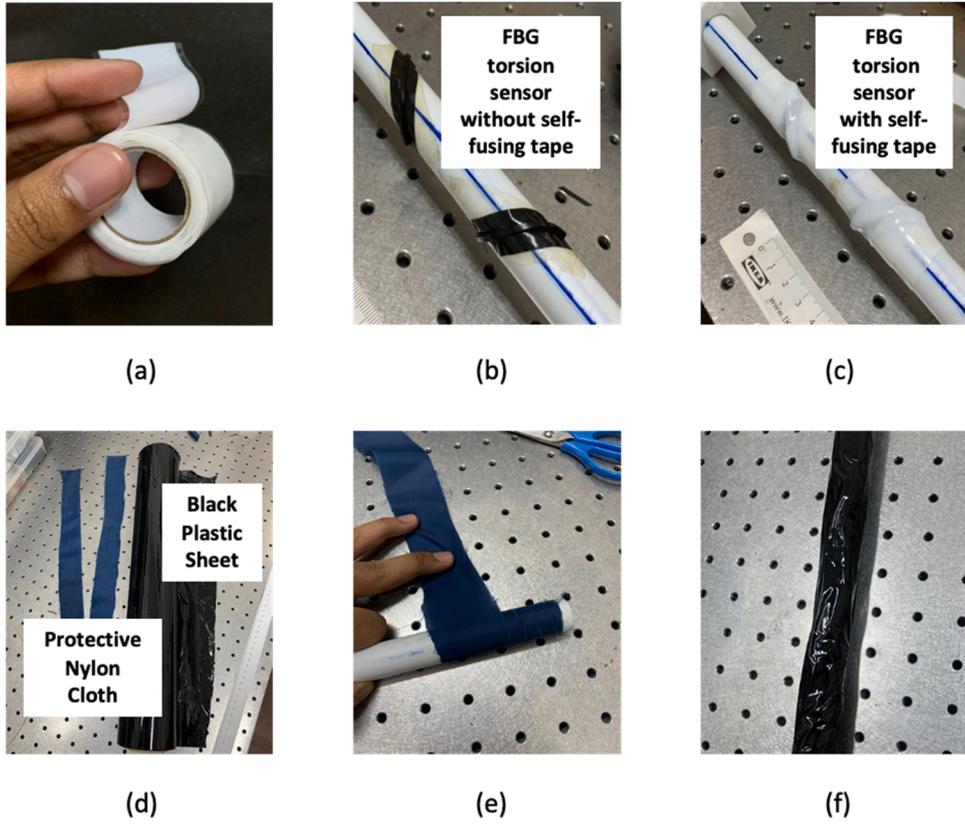
Fig. 5. Illustration of the actual picture of (a) WALTEK silicon self-fusing tape, (b) FBG torsion sensor without self-fusing tape, (c) FBG torsion sensor with self-fusing tape, (d) protective nylon cloth and black plastic sheet, (e) the winding scheme of protective nylon cloth, and (f) PVC pipe after wrapping with a black plastic sheet.
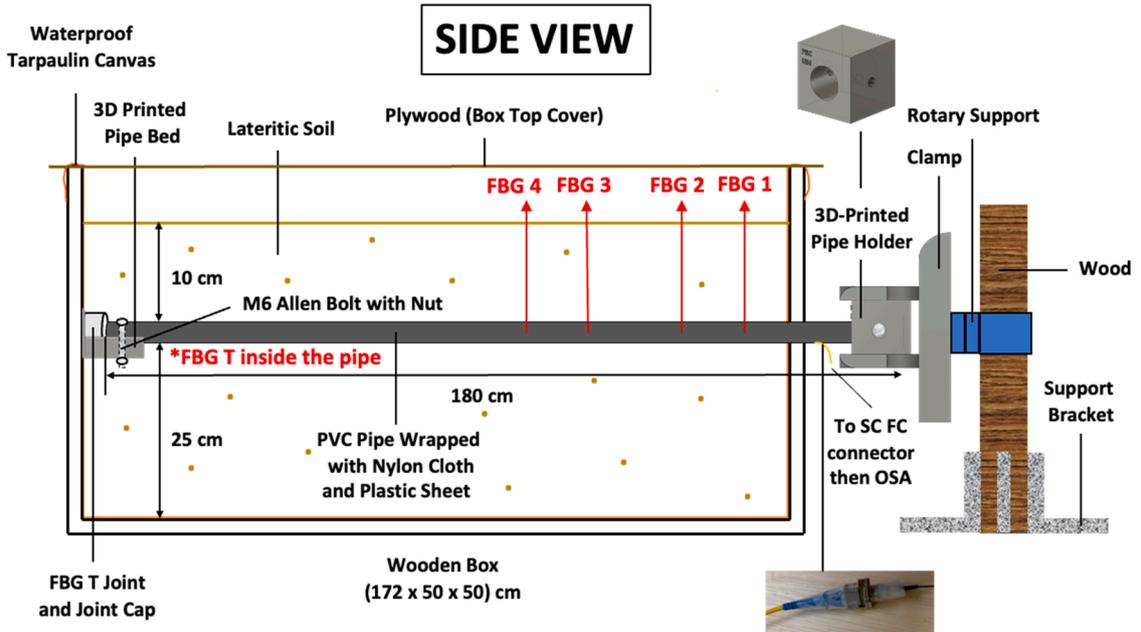

Fig. 6. Illustration of the field-testing setup for measurements of torsion in underground environments.

where the torsion strain of the PVC pipe is given by $\gamma = D\varphi/2l$, where D is the diameter of the PVC pipe, φ represents the angle of torsion of the free end of the PVC pipe and l is its length. If the torsion strain of the PVC pipe itself is small, the PVC pipe can be considered a uniform strain beam. Thus, the relationship between the Bragg wavelength shifts, λ_{Bn} (of all the n FBGs used), due to the strain experienced, ε_n, and the

changes in temperature, ΔT, can be expressed as [34]:

$$\Delta \lambda_{Bn} = P(K_{Sn}\varepsilon_n + K_{Tn}\Delta T), (n = 1, 2, 3 \text{ and } 4) \tag{4}$$

where K_{Sn} and K_{Tn} are the torsion sensor strain and temperature sensitivity, respectively, and P is a proportionality factor related to the bonding quality of the FBGs and the effective photoelastic coefficient of
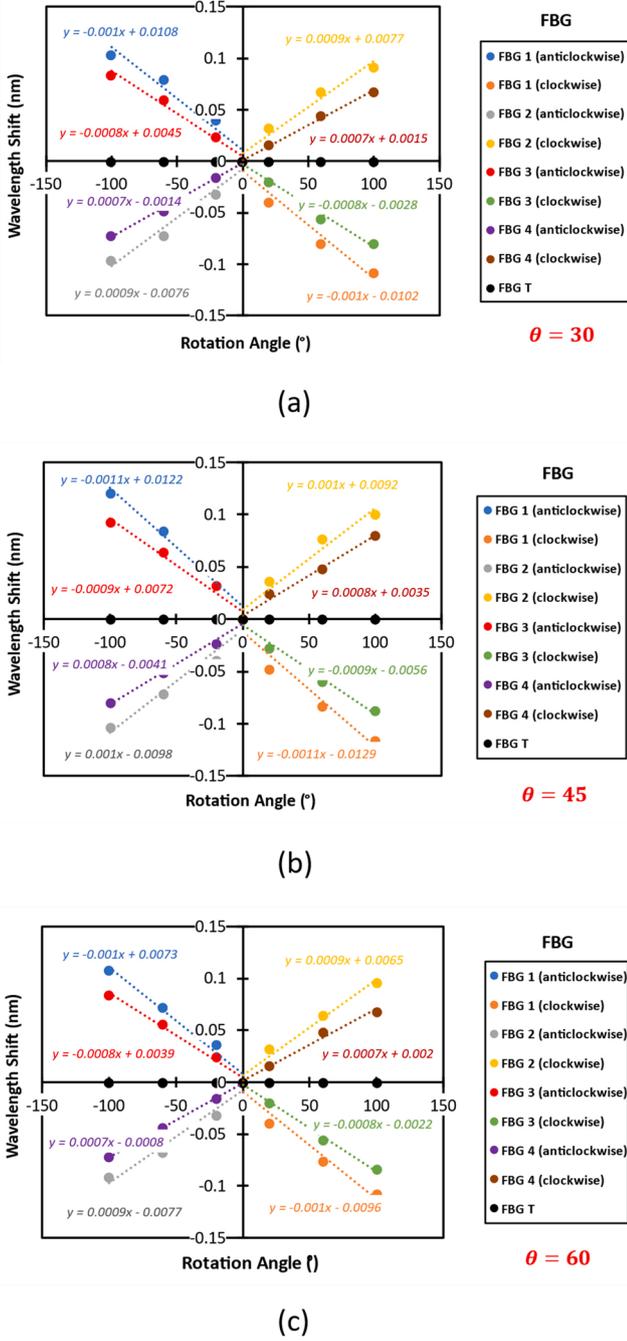
Fig. 7. Illustration of (a) the wavelength shift of all the FBGs used (including FBG T) in response to increasing torsion angle (showing 0°, 20°, 60°, and 100°) at a bonding angle of $\theta = 30°$, (b) $\theta = 45°$ and (c) $\theta = 60°$.

Fig. 8. Illustration of (a) the force distribution (measured in angles) at a bonding angle of $\theta = 30°$, (b) $\theta = 45°$ and (c) $\theta = 60°$.

3. Laboratory-based calibration of the FBG sensor

3.1. Setup for measurements of twist

The experimental setup used to evaluate the performance of the FBG-based sensor, based on the rotation at the free end of the pipe, is illustrated in Fig. 3. From the figure, the four strain-sensitive FBGs, each of different characteristic Bragg wavelengths, were bonded on one side of the pipe at an angle, θ, while an additional FBG that was used as a temperature compensator was placed loosely inside the pipe to allow only temperature measurements. Three stainless steel L brackets were used to avoid bending during testing. Table 2 shows the Bragg wavelengths, the angle of the FBG, and its position along the PVC pipe. As the length, L, and diameter, D, of the pipe are 100 cm and 6.4 cm, respectively, the torsion of the pipe and beam condition shows a good agreement (such that D/L << 1 [35,36]). One end of the PVC pipe was fixed on the optical table with an M6 Allen bolt, while the free end was positioned inside the 3D-printed pipe holder (made of PC filament due to its good hardness properties with an infill density of 30% and a grid infill pattern). The 3D-printed pipe holder contains a hole for the M6 Allen bolt to go through to fix the pipe inside it. Both ends of the pipe are drilled with holes of the same diameter as that of the M6 Allen bolts in a perpendicular arrangement, in which the fixed end is drilled at 90° from the z-axis of the optical table while the hole at the free end has a 90° difference (perpendicular) from the holes in the fixed end. Further, the rotating mechanism of the rotating clamp is marked in 10° intervals as a reference during measurements. Fig. 4(a) shows a photograph of the experimental setup used in this work.

A schematic diagram of the interrogation system employed is shown in Fig. 4(b). An amplified spontaneous emission (ASE) light source was connected to Port-1 of a 3-port circulator. Port-2 was connected to the optical fiber with the serially-spliced FBGs, while Port-3 was connected to a Yokogawa AQ6370C Optical Spectral Analyzer with a spectral range of 600–1700 nm, a wavelength resolution of 0.02 nm, accuracy of ± 0.01 nm, and a sampling frequency of 4000 Hz. This allows the response of the FBGs used to be measured. The experiments were conducted during the day over four days. The response of each strain-sensitive FBG in the system at different rotations was measured over

the fiber grating. It is important to note that the temperature sensitivities for all FBGs are assumed to be similar – a reasonable assumption given that it is located on the same PVC pipe (such that $K_{T1} = K_{T2} = K_{T3} = K_{T4}$ can be assumed for all strain-sensitive FBGs). Substituting Eq. 2 and Eq. 3 into Eq. 4 will give the wavelength shift for each of the FBGs, as shown below, where:

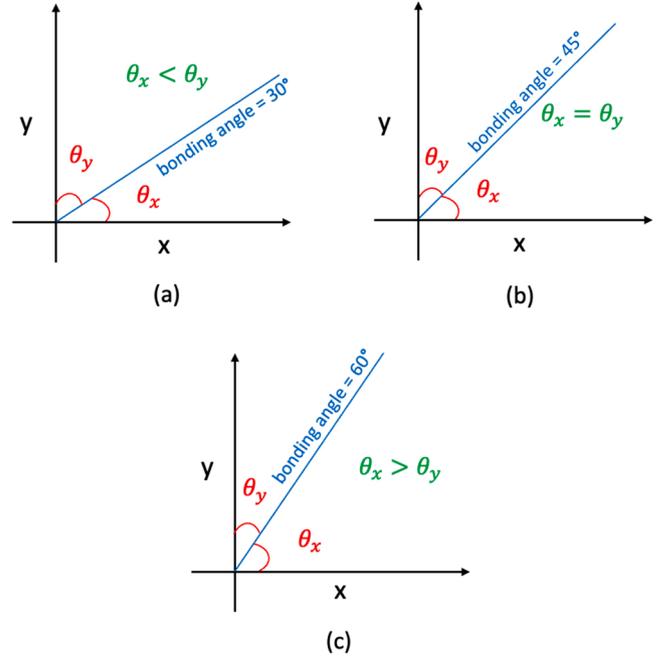$$\Delta\lambda_{Bn} = \frac{PD(\lambda_{Bn})(1 - p_{eff})\sin(2\theta)}{4L}\varphi \quad (5)$$

Table 4
The responsivity of each FBG (n = 1, 2, 3, and 4) and also FBG T, to increasing torsion angle when positioned at bonding angles of 30°, 45°, and 60°.

Bonding Angle (*θ*)	30°			45°		
FBG #	Clockwise Responsivity (pm/deg)	Anticlockwise Responsivity (pm/deg)	Average R^2	Clockwise Responsivity (pm/deg)	Anticlockwise Responsivity (pm/deg)	Average R^2
1	-1.0	1.0	0.9471	-1.1	1.1	0.9536
2	0.9	-0.9	0.9651	1.0	-1.0	0.9605
3	-0.8	0.8	0.9825	-0.9	0.9	0.9727
4	0.7	-0.7	0.9951	0.8	-0.8	0.9912
T	0.0	0.0	0.0000	0.0	0.0	0.0000
Bonding Angle (*θ*)	60°					
FBG #	Clockwise Responsivity (pm/deg)	Anticlockwise Responsivity (pm/deg)	Average R^2			
1	-1.0	1.0	0.9645			
2	0.9	-0.9	0.9651			
3	-0.8	0.8	0.9862			
4	0.7	-0.7	0.9879			
T	0.0	0.0	0.0000			

the range of −100° to +100° in a step of 10°. When the free end of the pipe was rotated in the counterclockwise direction, both FBG 1 and FBG 3 were stretched due to their positions along the pipe. However, by contrast, FBG 2 and FBG 4 were compressed as they were positioned away from the direction of rotation. The same approach was applied to all FBGs in the case of clockwise rotation. Since all FBGs are positioned at an angle, *θ*, along one side of the pipe, it is also essential to compare the response of the FBGs at different bonding angles. This is to determine the best bonding angle for the FBGs to obtain the most optimum outcome in torsion measurements. To perform this comparison, two additional experiments were conducted where the bonding angle of the FBGs was changed and presented in Table 3.

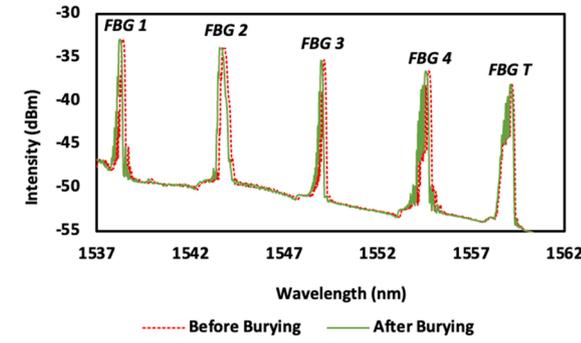### 3.2. Setup for field testing in soil movements environment

To ensure efficient and reliable performance of the embedded FBG torsion sensors during field testing, these FBGs need protection, as shown in Fig. 5(c). Therefore, a high-quality self-fusing silicon rubber tape manufactured by WALTEK, shown in Fig. 5(a), was applied due to its outstanding attributes, as it has impressive waterproofing and moisture resistance properties, has high flexibility and can operate in a wide range of temperatures (−60 °C to +200 °C). Furthermore, this tape can also form a watertight seal with an excellent instantaneous fusion to itself, making it well suited to seal materials in a wide range of applications. Pictures of the embedded FBG torsion sensors before and after the tape was applied can be seen in Fig. 5(b) and (c) respectively. Previously, Alias et al. [23] had also used the same tape to protect their FBG-based strain sensor which was embedded inside a 3D-printed TPU structure. By doing so, they have found that not only does this tape provide a watertight seal and protection for the embedded FBG sensors, but it also enhances the sensitivity of the sensor by ~1.13 times which proves that it can be applied effectively in the field applications. Then, a protective cloth made of nylon as seen in Fig. 5(d) was wrapped around the whole length of the PVC pipe, as shown in Fig. 5(e), to provide an additional waterproofing property to the FBG torsion sensors. Then, to ensure a smoother surface upon installation, an extra layer of the black plastic sheet as in Fig. 5(d) was applied to the outer section of the PVC pipe, as illustrated in Fig. 5(f), where the black plastic sheet also plays a role to prevent the soil moisture from affecting the device. Although there has been a report by Schenato *et. al* [37] using nylon instead of TPU to embed the FBG, but nylon has a higher Young's modulus, making them less elastic and flexible. For better sensitivity, using TPU wrapping with high-quality self-fusing silicon rubber tape will provide a better sensitivity and also water-proofing capability.

In order to evaluate the response of the FBG sensors during field testing, the PVC pipe containing the FBG sensors was laid horizontally inside a wooden box (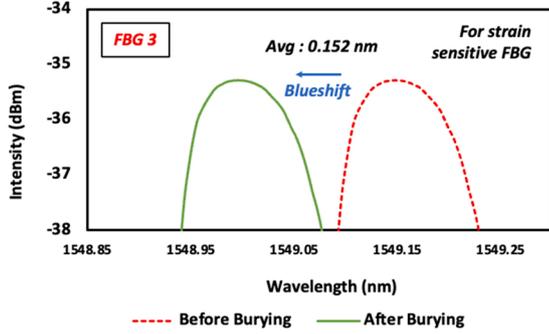of dimensions of 172 cm × 50 cm x 50 cm) filled with lateritic soil, as shown in Fig. 6. The wooden box was covered with an additional plywood to avoid any external force to be exerted on the surface of the soil. Since the soil was already compact, the pipe will not experience any bending, thus only allowing torsional measurement. Next, to allow torsion measurements to be evaluated, one end of the pipe was laid on a PLA-based 3D-printed pipe bed (screwed into the wood), and its position was fixed by an M6 Allen bolt that goes through the hole made at the pipe, and the pipe bed. Then, the other end of the pipe was fixed inside a PC-based pipe holder, similar to the setup illustrated in Fig. 3, to allow measurements of torsion to be made by the FBG sensors. The response of each of the FBGs used was measured in 10° intervals for both clockwise and counterclockwise directions over the range of −100° to +100°. In parallel to the setup shown in Fig. 3, FBG 1 and FBG 3 will be stretched, while FBG 2 and FBG 4 will be compressed when a counterclockwise rotation was applied at the free end of the pipe. A similar approach was applied to all FBGs in the case of clockwise rotation. One of the possible applications of this design is in landslide monitoring. Inclinometers and extensometers are typical devices used to monitor slope stability at a specific location by measuring ground displacement. At times, the unwanted rotation of these devices especially at the bottom cap which was fixed at the end of the borehole could cause errors in the measurement of ground displacement. As a result, this would trigger the early warning signal of the landslide monitoring system. This issue can be overcome by placing this device at the bottom end of the borehole, which can help to alleviate false warnings. Any slight rotation that occurs within the device can be determined, hence, correction can be made on the ground displacement as to provide an accurate and reliable reading.
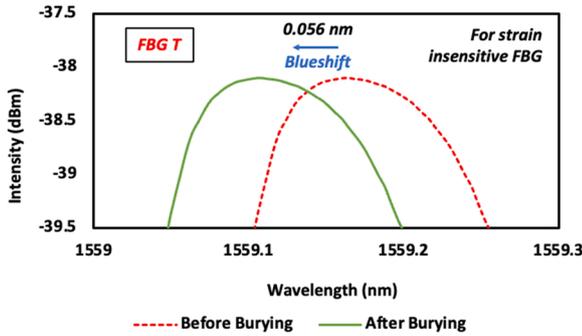
3.3. Temperature characterization

To ensure that FBG T is a reliable sensor for temperature and thus able to provide the compensation needed, a calibration of the FBG T was performed by placing the FBG sensor inside a pipe in a water bath, where the temperature is varied in a known manner. The water temperature in the water bath was initially set to room temperature, 25 °C, and slowly increased until a temperature of 50 °C was achieved. At the same time, the shift of the wavelength of FBG T was measured. Since the other strain-sensitive FBGs (FBG 1, FBG 2, FBG 3, and FBG 4) are positioned on the outer part of the PVC pipe, it is assumed that these FBGs were exposed to a different thermal exposition. Therefore, an additional calibration was performed on all strain-sensitive FBGs where the steps are mostly similar to the calibration of FBG T. The only difference is that all strain-sensitive FBGs were bonded on a short section of the PVC pipe instead of hanging loose inside. The response of all strain-sensitive FBGs was measured over the range of 25 °C to 50 °C.

Fig. 9. Illustration of the (a) wavelength spectra of all FBGs, (b) wavelength shift of FBG 3 (example of strain-sensitive FBG), and (c) wavelength shift of FBG T (strain-insensitive FBG) before and after being buried under the soil.
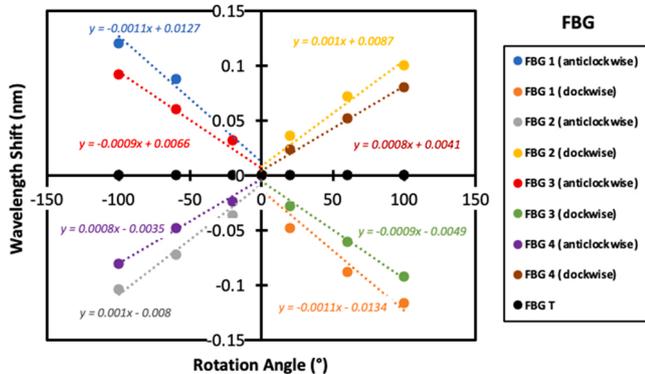

Fig. 10. Illustration of (a) the wavelength shift of all the FBGs used (including FBG T) in response to increasing torsion angle (showing 0°, 20°, 60°, and 100°).

Table 5
The responsivity of each FBG (n = 1, 2, 3, and 4) and also FBG T, to increasing torsion angle.

FBG #	Clockwise Responsivity (pm/deg)	Anticlockwise Responsivity (pm/deg)	Average R^2
1	-1.1	1.1	0.9492
2	1.0	-1.0	0.9736
3	-0.9	0.9	0.9877
4	0.8	-0.8	0.9912
T	0.0	0.0	0.0000

4. Results and discussion

4.1. Measurements of torsion (twist)

Fig. 7 illustrates the wavelength shift of all the FBGs used (including FBG T) as a function of increasing torsion angle, φ. From the figures, it can be observed that the wavelength shift for each strain-sensitive FBG differs due to its position along the pipe, such that $\Delta\lambda_{FBG1} > \Delta\lambda_{FBG2} > \Delta\lambda_{FBG3} > \Delta\lambda_{FBG4}$ for both directions of rotation (clockwise and anticlockwise). Compared to the other FBGs, FBG 1 shows the highest wavelength shift because it is positioned closer to the free end of the pipe, where the maximum rotation occurs. From Fig. 7(a), due to FBG 1 being positioned at an angle of 30° in the direction of anticlockwise rotation, the gratings of FBG 1 were stretched, thus causing its Bragg wavelength to be shifted to a higher wavelength, giving a red spectral shift. However, this is not the case when the pipe was rotated in a clockwise direction due to FBG 1 being positioned at an angle that points away from the clockwise direction. As a result, the gratings of FBG 1 were compressed, causing their Bragg wavelengths to move towards shorter wavelengths, giving a blue spectral shift.

The plot of the graphs in Fig. 7(b) and (c) also indicate a similar trend. However, the response of the FBGs was seen to be ~1.1 times higher when it is positioned at an angle of 45°. It is because the gratings of the FBGs experience equal force distribution in both the x and y-axis, as presented in Fig. 7(b), such that $\theta_x = \theta_y$. When the angle of bonding concerning both axes is equivalent, the torsional force experienced by the FBG's gratings during torsion measurement will be higher than when it is not. This will result in a better response from the FBGs, showing a greater wavelength shift to be measured when positioned at a bonding angle of 45° as in Fig. 7(b). It can be noted that the force distribution in Fig. 7(a) and (c) will not be equal when $\theta_x \neq \theta_y$ as in the case of $\theta_x < \theta_y$ and $\theta_x > \theta_y$ respectively. For these cases, the gratings of the FBG will not be able to obtain optimum response during torsion measurement, thus resulting in a less sensitive response from the FBGs. The response of the FBGs showing this manner can be seen in Fig. 7(a) and (c) for the case of both clockwise and anticlockwise rotation. The graph of force distribution in Fig. 8 was constructed so that the pipe was cut at its cross-section and laid flat on a smooth surface showing the bonding angle of the FBGs.

Table 4 shows the responsivity of all the strain-sensitive FBGs with increasing torsion angles when positioned at different bonding angles, validating the good linear fit obtained in Fig. 7. An average responsivity of 0.85 pm/deg for both the clockwise and anticlockwise directions was obtained when the FBG was bonded at an angle of 30° and 60°, with an average R^2 value of 0.9725 and 0.9759, respectively. However, a higher response of 0.95 pm/deg for both the clockwise and anticlockwise direction was achieved when the FBGs were bonded at 45°, with an average R^2 value of 0.9695, thus proving that the embedded FBG sensors can reliably be used to monitor torsion especially when it was bonded at an angle of 45°, forming the basis of a sensor system for use in field applications such as landslide monitoring and structural health monitoring.
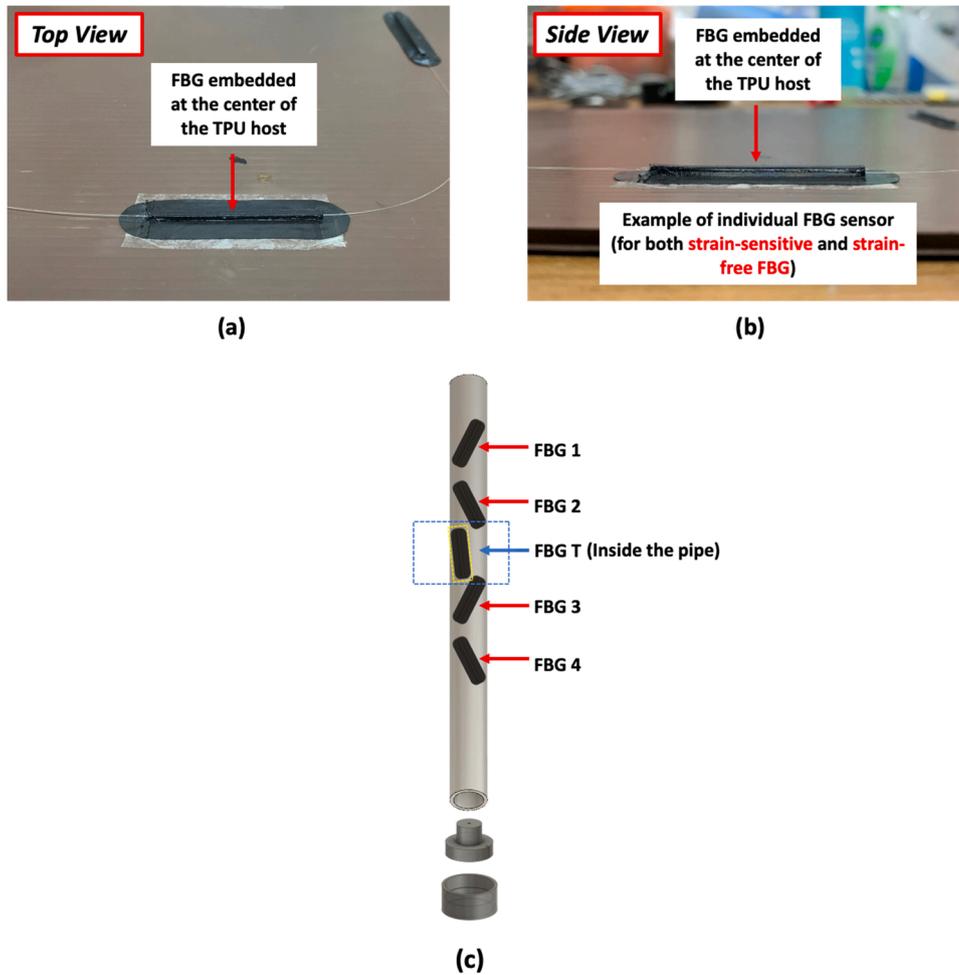
Fig. 11. Illustration of the (a) actual picture of the FBG sensor (for all FBGs: Strain-sensitive and strain-free) from a top view perspective, (b) side view perspective, and (c) its placement on the pipe with reference to Fig. 3, FBG T is held loosely inside the pipe and FBG 1, 2, 3 and 4 are being placed at the outer wall of the pipe.

4.2. Field testing in simulated soil condition

To assess the FBGs' response below the ground environments, the FBG-based sensor system was buried in the soil as shown earlier in Fig. 6. Fig. 9(a) shows the full wavelength spectra of all FBGs present in the system. The Bragg wavelength shifts of the strain-insensitive FBG, which is FBG T, are first measured before and after being buried in the soil. This was also done with the strain-sensitive FBG, where the wavelength shifts of FBG 3 are taken as an example. From Fig. 9(c), the strain-insensitive FBG, which is FBG T, experienced a blueshift of 0.056 nm after the FBG-based sensor system was buried in the soil. This is due to the decrease in the temperature experienced by FBG T when it is buried in the soil.

In the case of the strain-sensitive FBG, which is FBG 3, the Bragg wavelength was shifted to the left or blueshifted by as much as 0.152 nm as shown in Fig. 9(b). Since the Bragg wavelength shift of FBG 3 was higher compared to FBG T, it is suspected that the strain-sensitive FBG is affected by both temperature and strain variations, where the strain experienced by FBG 3 was caused by the weight of the soil acting towards the sensor. This is the same for all strain-sensitive FBGs, including FBG 1, FBG 2, and FBG 4, as the average blueshift measured was 0.152 nm. To allow the temperature effects for all strain-sensitive FBGs to be compensated, the wavelength shift for FBG T in Fig. 9(c), measured to be 0.056 nm, was subtracted off with the wavelength shift for all strain-sensitive FBGs obtained from the data in Fig. 9(b). This is to enable a precise measurement of strain to be measured by the strain-sensitive FBGs. As the gratings of FBG T are only sensitive to temperature changes due to their position inside the pipe, FBG T can be made as

a reliable temperature sensor to provide compensation for the other strain-sensitive FBGs (FBG 1, 2, 3, and 4), if there are any temperature variations. Fig. 10 presents the Bragg wavelength shift of all FBGs (including FBG T) in response to increasing torsion angle, φ.

Based on Fig. 10, a similar trend can be observed to the results obtained in Fig. 7 in the case of laboratory testing, where each of the strain-sensitive FBGs has a different response towards increasing torsion angle. This further shows that the Bragg wavelength shift experienced by FBG 1, FBG 2, FBG 3, and FBG 4 were dissimilar since they were placed at different positions and bonding angles along the pipe. Due to FBG 1 being closer to the free end of the pipe and positioned at 45°, it will experience more rotation (in the counterclockwise direction) compared to FBG 3, which was positioned at a similar bonding angle (45°) but further from the free end. This results in a higher wavelength shift to be obtained by FBG 1 as its gratings will be stretched more than that of FBG 3, causing a redshift to be experienced. It is also worth noting that since FBG T in Fig. 10 does not experience any wavelength shift, it can be said that all the strain-sensitive FBGs were only affected by strain variation.

Table 5 presents the response for all FBGs when positioned at different bonding angles in underground environments, showing an average responsivity of 0.95 pm/deg for both clockwise and anticlockwise rotation with high linearity of up to 99%. The average response of the FBGs was similar to that in Fig. 7(b), validating a good response for all FBGs thus proving that the embedded FBG sensors can be applied effectively for use in buried applications.
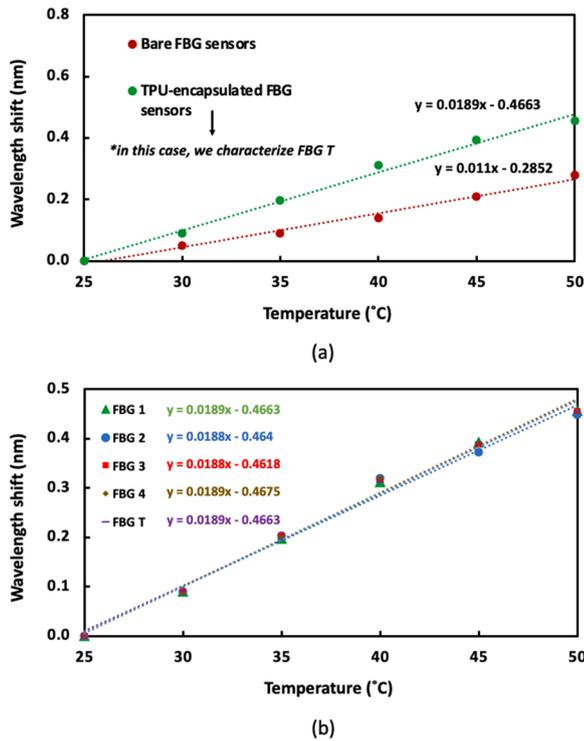
Fig. 12. Illustration of the temperature sensitivity of (a) bare and TPU-encapsulated FBG (FBG T) and (b) strain-sensitive FBGs (FBG 1, FBG 2, FBG 3, and FBG 4) and FBG T.

4.3. Temperature characterization

Fig. 11 illustrates the embedded FBG 1, 2, 3, 4, and also FBG T, whereby Fig. 11(a) provides a top view of the embedded FBG in the TPU host and Fig. 11(b) gives the side view of the sensor structure. Fig. 11(c) provides a schematic diagram of the PVC pipe with FBG 1, 2, 3, and 4 being bonded on the outer wall of the pipe. FBG T was being sandwiched between FBG 1, 2 and FBG 3, 4. This was done to ensure the FBG T detects the wavelength shift due to the temperature change.

It is also important to perform temperature characterization of the FBG sensors designed for torsion measurement and temperature compensation, to ensure their reliability over a wide range of temperatures. Since all FBGs were embedded at the center of a TPU material, a comparison of temperature sensitivity with a bare FBG was done and shown in Fig. 12(a). In this case, FBG T was taken as the reference since the placement of FBG T inside the pipe allows temperature correction to be performed on all strain-sensitive FBGs. Based on Fig. 12(a), the temperature sensitivities between the bare and TPU-encapsulated FBGs are 11.0 pm/°C and 18.9 pm/°C, respectively. The higher temperature sensitivity obtained by the TPU-encapsulated FBG sensor was due to the larger thermal expansion of the TPU material, which induces strain on the FBG. Furthermore, as the other strain-sensitive FBGs were placed at the outer surface of the pipe, factors such as thermal exposition must be considered. FBG T was not affected by the strain which was being held loosely inside the pipe to provide the temperature compensation. In this aspect, we have experimented to determine the temperature sensitives of the strain-sensitive FBGs and FBG T with different exposure. Since the strain-sensitive FBGs (FBG 1, FBG 2, FBG 3, and FBG 4) were positioned at different outer parts of the PVC pipe, it was assumed that these FBGs were exposed to a different thermal exposition.

Therefore, an additional calibration was performed on all strain-sensitive FBGs where the steps were mostly similar to the calibration of FBG T. The only difference was that all strain-sensitive FBGs were bonded on a short section of the PVC pipe instead of hanging loose inside the pipe. The response of all strain-sensitive FBGs was measured over the range of 25–50 °C. From the measurement, the temperature dependence of the strain-sensitive FBGs gives nearly the same value as the FBG T inside the PVC pipe. From Fig. 12(b), the temperature sensitivities for FBG 1, 2, 3, and 4 are 18.90, 18.80, 18.80, and 18.90 pm/°C, respectively. Thus, the average temperature sensitivity for the four FBGs will be 18.85 pm/°C. In the case of FBG T, it has a temperature sensitivity of 18.90 pm/°C. This gives a small difference between the two measurements of 0.05 pm/°C.

The coefficient of thermal expansion (CTE) of the thermoplastic polyurethane 95 A (TPU95A) has a higher value compared to the PVC pipe and the silica glass, which is the lowest. The CTE for TPU95A is 100.0×10^{-6} m.°C^{-1} [38], which is 2 times higher than the CTE of PVC pipe (supporting material) with a value of 50.4×10^{-6} m.°C^{-1} [39]. The CTE for silica glass is 0.5×10^{-6} m.°C^{-1} [31,40,41]. The FBG T was also embedded in the TPU similarly to FBG 1, 2, 3, and 4. Therefore, when the temperature increases from 25–50 °C, the TPU expands at a higher rate compared to PVC pipe and silica glass. As such, the expansion due to the PVC pipe can be neglected because most of the expansion comes from the TPU which is more dominant. The wavelength shift due to temperature for the case of FBG 1–4 will be offset by the reading of the FBG T that is also embedded in a similar TPU structure. Therefore, FBG 1, 2, 3, and 4 will only measure the strain from the soil to the pipe.

5. Conclusion

In this work, a fiber optic sensor system, designed using FBGs and 3D-printing technology was presented for the measurement of torsion. The embedment of the FBGs inside a thermoplastic polyurethane material had proven to be a reliable and inexpensive way to fabricate the sensor system, in which the infill density is set at 20% with a concentric infill pattern. This infill setting provides good flexibility and strength in the printed output thus allowing a reliable measurement of torsion in which the results obtained have shown a promising average responsivity of 0.95 pm/deg for both clockwise and anticlockwise rotations, with linearity values of up to 99% when the FBG was bonded at the pipe with an angle of 45°. The sensor system had incorporated an additional FBG (labeled FBG T) to operate as a temperature sensor (with a temperature sensitivity of 18.90 pm/°C) and as FBG T was not affected by strain variations, it can be used efficiently to provide compensation for the whole sensor system. This work had also shown good results when tested in underground environments, giving an average responsivity of 0.95 pm/deg for both clockwise and anticlockwise rotations, with linearity values of up to 99%. The system had been designed to be applied in a range of engineering applications such as structural health monitoring of buildings or landslides and in-the-filed validation of the sensor performance in the subject of ongoing work.

References

[1] C. Hong, Y. Zhang, Z. Lu, Z. Yin, A FBG tilt sensor fabricated using 3D printing technique for monitoring ground movement, IEEE Sens. J. 19 (15) (2019) 6392–6399, https://doi.org/10.1109/JSEN.2019.2908873.

[2] A. Huang, C.C. Wang, J.T. Lee, Y. Ho, Applications of FBG-based sensors to ground stability monitoring, J. Rock. Mech. Geotech. Eng. 8 (4) (2016) 513–520, https://doi.org/10.1016/j.jrmge.2016.01.007.

[3] C.Y. Hong, Y.F. Zhang, M.X. Zhang, L.M.G. Leung, L.Q. Liu, Application of FBG sensors for geotechnical health monitoring, a review of sensor design, implementation methods and packaging techniques, Sens. Actuators A Phys. 244 (2016) 184–197, https://doi.org/10.1016/j.sna.2016.04.033.

[4] H. Tian, D. Liu, Y. Wang, Q. Wang, Effect of adhesive type on the sensitivity coefficient of FBG sensor bonded on the surface of CFRP, Optoelectron. Lett. 15 (4) (2019) 264–268, https://doi.org/10.1007/s11801-019-8183-5.

[5] Z. Lu, C. Hong, Y. Zhang, D. Su, Y. Fu, Development of an FBG sensor for measuring large range and multi-directional settlement, IEEE Photonics J. 7 (8) (2019) 669–677, https://doi.org/10.1109/ACCESS.2019.2932774.

[6] N. Tanaka, Y. Okabe, N. Takeda, Temperature-compensated strain measurements using FBG sensors embedded in composite laminates, Smart Struct. Mater. Smart Sens. Technol. Meas. Syst. 4694 (2002) 304–313, https://doi.org/10.1117/12.472634.

[7] Y. Hu, C. Hong, Y. Zhang, G. Li, A monitoring and warning system for expressway slopes using FBG sensing technology, Int. J. Distrib. Sens. Netw. 14 (5) (2018), https://doi.org/10.1177/1550147718776228.

[8] W. Li, C. Xu, S.C.M. Ho, B. Wang, G. Song, Monitoring concrete deterioration due to reinforcement corrosion by integrating acoustic emission and FBG strain measurements, J. Sens. 17 (3) (2017) 1–12, https://doi.org/10.3390/s17030657.

[9] S.F. Jiang, Z.H. Qiao, N.L. Li, J. Luo, Structural health monitoring system based on FBG sensing technique for Chinese ancient timber buildings, J. Sens. 20 (1) (2020) 1–17, https://doi.org/10.3390/s20010110.

[10] J. Frieden, J. Cugnoni, J. Botsis, T. Gmür, D. Ćorić, High-speed internal strain measurements in composite structures under dynamic load using embedded FBG sensors, Compos. Struct. 92 (8) (2010) 1905–1912, https://doi.org/10.1016/j.compstruct.2010.01.007.

[11] H.H. Zhu, B. Shi, C.C. Zhang, FBG-based monitoring of geohazards: current status and trends, Sens. Actuators A Phys. 296 (1) (2017) 132–144, https://doi.org/10.3390/s17030452.

[12] A. Huang, C.C. Wang, J.T. Lee, Y. Ho, Applications of FBG-based sensors to ground stability monitoring, J. Rock. Mech. Geotech. Eng. 8 (4) (2016) 513–520, https://doi.org/10.1016/j.jrmge.2016.01.007.

[13] W. Zhang, G. Kai, X. Dong, S. Yuan, Q. Zhao, Temperature-independent FBG-type torsion sensor based on combinatorial torsion beam, IEEE Photonics Technol. Lett. 14 (8) (2002) 1154–1156.

[14] L. Yan, Z. Wu, Z. Zhang, W. Pan, B. Luo, P. Wang, High-speed FBG-based fiber sensor networks for semi distributed strain measurements, IEEE Photonics J. 5 (2) (2013) 1–7, https://doi.org/10.1109/JPHOT.2013.2258143.

[15] Y. Zhang, L. Borana, Design, fabrication and testing of a 3D printed FBG pressure sensor, IEEE Access 7 (10) (2019) 38577–38583, https://doi.org/10.1109/ACCESS.2019.2905349.

[16] O. Frazão, L.A. Ferreira, F.M. Araújo, J.L. Santos, Simultaneous measurement of strain and temperature using fibre Bragg gratings in a twisted configuration, J. Opt. A Pure Appl. Opt. 7 (8) (2005) 427–430, https://doi.org/10.1088/1464-4258/7/8/014.

[17] S.C. Her, W.N. Lin, Simultaneous measurement of temperature and mechanical strain using a fiber Bragg grating sensor, J. Sens. 20 (15) (2020) 1–12, https://doi.org/10.3390/s20154223.

[18] R. Li, Y. Tan, Y. Chen, L. Hong, Z. Zhou, Investigation of sensitivity enhancing and temperature compensation for fiber Bragg grating (FBG)-based strain sensor, no. November 2018, Opt. Fiber Technol. 48 (2019) 199–206, https://doi.org/10.1016/j.yofte.2019.01.009.

[19] V. Mishra, M. Lohar, A. Amphawan, Improvement in temperature sensitivity of FBG by coating of different materials, Optik 127 (2) (2016) 825–828, https://doi.org/10.1016/j.ijleo.2015.10.014.

[20] L. Xu, N. Liu, J. Ge, X. Wang, M.P. Fok, Stretchable fiber-Bragg-grating-based sensor, Opt. Lett. 43 (11) (2018) 2503, https://doi.org/10.1364/ol.43.002503.

[21] X. Chen, K. Zhou, L. Zhang, I. Bennion, In-fiber twist sensor based on a fiber Bragg grating with 81° tilted structure, IEEE Photonics Technol. Lett. 18 (24) (2006) 2596–2598, https://doi.org/10.1109/LPT.2006.887371.

[22] N.N. Ismail, A.S. Sharbirin, M.S.M. Sa'ad, M.K.A. Zaini, M.F. Ismail, G. Brambilla, B.M.A. Rahman, K.T.V. Grattan, H. Ahmad, Novel 3D-printed biaxial tilt sensor based on fiber Bragg grating sensing approach, Sens. Actuators A Phys. 330 (2021), https://doi.org/10.1016/j.sna.2021.112864.

[23] M.A. Alias, M.F. Ismail, M.S.M. Sa'ad, M.K.A. Zaini, K.S. Lim, K.T.V. Grattan, G. Brambilla, B.M.A. Rahman, S.A. Reduan, H. Ahmad, A High-precision extensometer system for ground displacement measurement using fiber Bragg grating, IEEE Sens. J. 22 (9) (2022) 8509–8521, https://doi.org/10.1109/JSEN.2022.3159850.

[24] D. Lo Presti, C. Massaroni, C. Leitao, M.F. Domingues, M. Sypabekova, D. Barrera, I. Floris, L. Massari, C. Oddo, S. Sales, I. Iordachita, D. Tosi, E. Schena, Fiber bragg gratings for medical applications and future challenges: a review, IEEE Access 8 (2020) 156863–156888, https://doi.org/10.1109/ACCESS.2020.3019138.

[25] C. Tavares, C. Leitao, D. Lo Presti, M.F. Domingues, N. Alberto, H. Silva, P. Antunes, Respiratory and heart rate monitoring using an FBG 3D-printed wearable system, Biomed. Opt. Express 13 (4) (2022) 2299–2311, https://doi.org/10.1364/boe.452115.

[26] D. Lo Presti, C. Massaroni, J. D'Abbraccio, L. Massari, M. Caponero, U.G. Longo, D. Formica, C. Oddo, E. Schena, Wearable system based on flexible FBG for respiratory and cardiac monitoring, IEEE Sens. J. 19 (2019) 7391–7398, https://doi.org/10.1109/JSEN.2019.2916320.

[27] M. Majumder, T.K. Gangopadhyay, A.K. Chakraborty, K. Dasgupta, D. K. Bhattacharya, Fibre Bragg gratings in structural health monitoring - present status and applications, Sens. Actuators A Phys. 147 (1) (2008) 150–164, https://doi.org/10.1016/j.sna.2008.04.008.

[28] H. Ahmad, M.A. Alias, M.F. Ismail, N.N. Ismail, M.K.A. Zaini, K.S. Lim, G. Brambilla, K.T.V. Grattan, B.M.A. Rahman, Strain sensor based on embedded fiber Bragg grating in thermoplastic polyurethane using the 3D printing technology for Improved Sensitivity, Photon. Sens. 12 (3) (2022), https://doi.org/10.1007/s13320-021-0646-1.

[29] Y.L. Wang, B. Shi, T.L. Zhang, H.H. Zhu, Q. Jie, Q. Sun, Introduction to an FBG-based inclinometer and its application to landslide monitoring, J. Civ. Struct. Health Monit. 5 (5) (2015) 645–653, https://doi.org/10.1007/s13349-015-0129-4.

[30] M.G. Zubel, K. Sugden, D.J. Webb, D. Sáez-Rodríguez, K. Nielsen, O. Bang, Embedding silica and polymer fibre Bragg gratings (FBG) in plastic 3D-printed sensing patches, in: Proceedings of SPIE, Micro-Structured and Specialty Optical Fibres IV, vol. 9886, pp. 1–12, 2016, doi: 10.1117/12.2228753.

[31] N.F. Razali, M.H. Abu Bakar, N. Tamchek, M.H. Yaacob, M.A. Mahdi, Temperature sensitivity comparison between bare FBG and buffered FBG, in: Proceedings of ICP 2014: 5th International Conference on Photonics 2014, Kuala Lumpur, vol. 14, pp. 36–37, 2014, doi: 10.1109/ICP.2014.7002303.

[32] C. Li, W. Yang, M. Wang, X. Yu, J. Fan, Y. Xiong, Y. Yang, L. Li, A review of coating materials used to improve the performance of optical fiber sensors, Sensors 20 (15) (2020) 1–24, https://doi.org/10.3390/s20154215.

[33] A.G. Leal-Junior, C. Marques, M.R.N. Ribeiro, M.J. Pontes, A. Frizera, FBG-embedded 3-D printed ABS sensing pads: the impact of infill density on sensitivity and dynamic range in force sensors, IEEE Sens. J. 18 (20) (2018) 8381–8388, https://doi.org/10.1109/JSEN.2018.2866689.

[34] L. Fang, T. Chen, R. Li, S. Liu, Application of embedded fiber Bragg grating (FBG) sensors in monitoring health to 3D printing structures, IEEE Sens. J. 16 (17) (2016) 6604–6610, https://doi.org/10.1109/JSEN.2016.2584141.

[35] W.G. Zhang, Z.G. Wu, Y.G. Liu, Y.F. Yang, G. Kai, Q.D. Zhao, S. Yuan, X. Dong, E. Li, J. Xi, J. Chicharo, Principles and realizations of FBG wavelength tuning with elastic beams, Optoelectron. Lett. 1 (1) (2005) 5–9.

[36] W. Zhang, Q. Tu, E. Li, J. Xi, J. Chicharo, G. Kai, S. Yuan, X. Dong, Temperature-independent FBG-type torsion sensor, in: Passive Components and Fiber-based Devices II, 2005, vol. 6019, p. 601919. doi: 10.1117/12.634919.

[37] L. Schenato, Q. Rong, Z. Shao, X. Quiao, A. Pasuto, A. Galtarossa, L. Palmieri, Highly sensitive FBG pressure sensor based on a 3D-printed transducer, J. Light. Technol. 37 (18) (2019) 4784–4790, https://doi.org/10.1109/JLT.2019.2919917.

[38] Ultimaker, "Technical datasheet TPU95A," Version 3.010 datasheet, May 2017.

[39] "Piping materials - temperature expansion coefficients," Engineering ToolBox, 2003. [Online]. Available: ⟨https://www.engineeringtoolbox.com/pipes-temperature-expansion-coefficients-d_48.html⟩.

[40] K. Cho, S.T. Kim, Y.H. Park, J.R. Cho, Measurement of mechanical and thermal strains by optical FBG sensors embedded in CFRP rod, J. Sens. 2019 (2019), https://doi.org/10.1155/2019/5345901.

[41] T.S. Hsieh, Y.C. Chen, C.C. Chiang, Analysis and optimization of thermodiffusion of an FBG sensor in the gas nitriding process, Micromachines 7 (12) (2016), https://doi.org/10.3390/mi7120227.

M.A. Alias received the Bachelor of Science (Hons) in Industrial Physics from the Faculty of Science, Universiti Teknologi Malaysia (UTM), Johor, Malaysia in 2020. He is currently a postgraduate student and a research assistant at Photonics Research Centre, Universiti Malaya, Kuala Lumpur, Malaysia. His current research interest focuses on optical fiber sensors mainly on fiber Bragg grating.

K.T.V. Grattan graduated in Physics from Queen's University Belfast with a BSc (First Class Honours) in 1974, followed by a Ph.D. in Laser Physics. His doctoral research involved the use of laser-probe techniques for measurements on potential new laser systems. He obtained the degree of Doctor of Science (DSc) from City University in 1992 for his sensor work. His research interests have expanded to include the development and use of fiber optic and optical systems in the measurement of a range of physical and chemical parameters.

H. Ahmad received the Ph.D. degree in laser technology from the University of Wales, Swansea, U.K., in 1983. He is currently a Professor with the Department of Physics and director of the Photonics Research Centre, Universiti Malaya, Kuala Lumpur, Malaysia, where he has actively pursued research activities in the field of photonics since 1983. He is the author of more than 400 professional papers in international journals and conference proceedings. His research interests are in lasers, fiber-based devices for telecommunications, and fiber-based sensor devices. Dr. Ahmad is a Fellow of the Academy of Sciences, Malaysia.

B.M.A. Rahman received BSc Eng. and MSc Eng. degrees in Electrical Engineering with distinctions from Bangladesh University of Engineering and Technology (BUET), Dhaka, Bangladesh, in 1976 and 1979, respectively He received his PhD degree in Electronic Engineering from University College, London in 1982. From 1976–1979, he was a Lecturer at the Electrical Engineering Department, BUET. In 1988, he joined the Electrical, Electronic and Information Engineering Department of City University, London, as a Lecturer, where he is now a professor. At City University, London, he leads the research group on Photonics Modelling, specialized in the development and use of the rigorous and full-vectorial numerical approaches, frequency domain modal solution approach, the beam propagation method, and time-domain approach, primarily based on the numerically efficient finite element method.

M.Z. Samion obtained his Bachelor of Engineering (Electrical) from the Faculty of Engineering, Universiti Malaya, Kuala Lumpur, Malaysia in 2015 and his Doctor of Philosophy (PhD) in Photonics Engineering in 2021. He is a research officer at the Photonics Research Centre, Universiti Malaya. His research focuses on pulsed and multiwavelength fiber lasers.

G. Brambilla is a professor at the Optoelectronics Research Centre and, since 2016, co-Director and General Manager of the Future Photonics Hub. He has been Director of the Centre for Innovative Manufacturing in Photonics until 2015. He obtained his MSc (Engineering) with honors from Politecnico di Milano (Italy) in 1996 and his PhD degree in Optoelectronics from the University of Southampton in 2002. In 2007 he was awarded the Royal Society Research Fellowship, which was then extended in 2012. His research interests include optical fiber sensors; optical fiber structuring using fs lasers; specialty and polymer fibers; new fiber fabrication technologies; UV fiber lasers; devices based on optical fiber nanowires, fiber tapers and couplers; rare earth doped scintillating fibers and fibers for nuclear sensing.

M.S.M. Sa'ad received the Bachelor of Science (Hons) in Pure Physics from the Faculty of Science, Universiti Malaya, Kuala Lumpur, Malaysia in 2019. He is currently a postgraduate student and a research assistant at the Photonics Research Centre, Universiti Malaya, Kuala Lumpur, Malaysia. His research interest focuses on fiber optic sensors mainly on fiber Bragg gratings.

M.K.A. Zaini received the bachelor's degree from the Department of Physics, Faculty of Science, University Putra Malaysia, Selangor, Malaysia, in 2015, and currently a postgraduate candidate at Photonics Research Centre, Universiti Malaya, Kuala Lumpur, Malaysia. His current research interest includes fiber Bragg grating sensors, and Spatial Division Multiplexing.

K.S. Lim received his Bachelor of Engineering degree from the Department of Electrical Engineering, Faculty of Engineering, Universiti Malaya, Kuala Lumpur. Malaysia, in 2008, and the Ph.D. degree from the Photonics Research Centre, Department of Physics, University of Malaya, in 2012. He is currently a Senior Lecturer with Photonics Research Centre, Universiti Malaya. His current research interests include fiber Bragg grating sensors, spatial division multiplexing, and laser medical devices. He is a Corporate Member of the Institute of Engineers Malaysia (IEM), a registered Professional Engineer (Telecommunication) of the Board of Engineers Malaysia (BEM), and a member of OSA.

L. Bayang received the B.Eng. degree from the Universiti Malaya in 2006, and the M.Eng. degree in 2015. He is currently a Science Officer with Photonics Research Centre, Universiti Malaya. He had coauthored numerous ISI professional articles and presented his work in many conferences. His current research interests include equipment test and measurement and the development of fast and ultra-fast fiber lasers.

M.F. Ismail obtained his Bachelor of Engineering (Telecommunication) from the Faculty of Engineering, Universiti Malaya, Kuala Lumpur, Malaysia in 1999 and Master of Engineering (Science) from the Faculty of Engineering, Universiti Malaya in 2004. He obtained his Ph.D. from the same university in 2021 where his research focuses on pulsed, multiwavelength fiber lasers and waveguide.